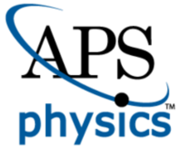

CHORUS

This is the accepted manuscript made available via CHORUS. The article has been published as:

Sputtering of Si_{c}Ge_{1−c} nanospheres

Herbert M. Urbassek, Maureen L. Nietiadi, R. Mark Bradley, and Gerhard Hobler

Phys. Rev. B **97**, 155408 — Published 10 April 2018

DOI: 10.1103/PhysRevB.97.155408

Sputtering of Si_cGe_{1-c} nanospheres

Herbert M. Urbassek,[1, *] Maureen L. Nietiadi,[1] R. Mark Bradley,[2] and Gerhard Hobler[3]

[1] *Physics Department and Research Center OPTIMAS, University Kaiserslautern, Erwin-Schrödinger-Straße, D-67663 Kaiserslautern, Germany*

[2] *Department of Physics, Colorado State University, Fort Collins, Colorado 80523, USA*

[3] *Institute of Solid-State Electronics, TU Wien, Floragasse 7, A-1040 Wien, Austria*

(Dated: March 29, 2018)

It is known that sputter yields of elemental materials depend on the target curvature. Here we explore to what extent this effect is modified for alloy targets using both Monte Carlo and molecular dynamics simulations. For the exemplary case of amorphous Si_cGe_{1-c} spheres, we find that, in the limit of small curvatures, the curvature dependence of the sputter preferentiality is negligible. This finding can be explained by a natural extension of the existing analytical theory of curvature-dependent sputtering for elemental materials. For large curvatures, however, the sputter preferentiality strongly depends on curvature. In this case, molecular-dynamics simulations also predict strong spike effects which increase the sputter yields. Sputter yield amplification – an increase in partial sputter yield with decreasing concentration of the element – occurs for Si-rich alloys.

PACS numbers: 79.20.Rf, 79.20.Ap, 61.80.Lj
Keywords: sputtering, nanoparticles, curvature, Monte Carlo simulation, molecular dynamics simulation

I. INTRODUCTION

Sputtering depends on the surface curvature [1, 2]. For a convex surface, the sputter yield is greater than for a flat surface. The increase in sputter yield may be pronounced if the curvature radius is of the order of the energy deposition depth; for considerably smaller curvature radii the yield decreases again. This effect has been investigated for the sputtering of nanospheres [3–10] and nanowires [11–16]. It is of obvious relevance for the sputtering of nanoparticles that are supported [17–19], that are in aerosols [20] or are in a plasma environment [21].

Curvature-dependent sputtering is also relevant for nanostructured or nanopatterned surfaces. Such surfaces may be created by the irradiation process itself, and so a knowledge of how the resulting surface patterns modify the sputter yield locally is important in theories of ion-induced patterning [22].

Elemental targets were considered in most previous studies. However, real targets are often alloys or compounds. Sputtering of non-elemental targets is made more complex by the phenomenon of preferential sputtering, i.e., the deviation of the partial sputter yields of the elements from proportionality to their respective surface concentrations. Further complications arise, since surface concentrations (i) may differ from the bulk values, and (ii) may change with fluence if the sputtering is preferential [23–25]. The effects of preferential sputtering may be strong, and thus it may be asked whether the effects of preferential sputtering will overshadow curvature effects in the sputtering of non-elemental targets.

The answer to this question is important in theories of the nanoscale patterns that emerge when the initially flat surface of a binary material is bombarded with a broad noble gas ion beam [26–28]. Interest in this kind of pattern formation burgeoned when it was discovered that when a planar surface of GaSb is bombarded with a normally-incident argon ion beam, a pattern of nanodots with a surprising degree of hexagonal order can form spontaneously on the surface [29]. If a comprehensive theory of this fascinating kind of pattern formation is to be developed, a more complete understanding of sputtering from nanostructured binary materials will be needed.

In this paper, we investigate the relative importance of curvature-dependent sputtering and preferential sputtering in binary materials using the completely miscible amorphous Si_cGe_{1-c} system as a prototypical example, thus extending previous detailed studies on the elemental Si system [9, 15]. We use Monte Carlo (MC) simulations as our main tool, since it combines well defined simulation conditions with computational speed. For small spheres, and also for flat targets, we perform additional molecular dynamics (MD) simulations that allow us to include attractive interactions and also many-body collision events, and thus the occurrence of collision spikes, in the targets. Finally, we will present an analytical model of the curvature dependence of sputtering for binary targets valid in the limit of large curvature radii; the assumptions underlying this theory will also be assessed here.

*Electronic address: urbassek@rhrk.uni-kl.de; URL: http://www.physik.uni-kl.de/urbassek/

II. SIMULATION METHODS

A. Monte Carlo

MC simulations in the binary collision approximation are performed with the IMSIL code in its static mode [30, 31] assuming amorphous targets. As the interatomic potential the pair-specific Ziegler-Biersack-Littmark (ZBL) potential [32] is used for the Si-Si interactions and the universal ZBL potential [32] otherwise. Electronic stopping is disregarded in this study, since there are uncertainties related to the electronic stopping in insulating or semiconducting targets [33]. Note, however, that electronic stopping might introduce a source of preferential energy transfer to the species of an alloy that we will not further investigate here. Moreover, we wish to compare our MC results with the MD simulations which are also performed without consideration of electronic stopping.

For details on the selection of collision partners and the treatment of the surface we refer the reader to our recent publications [34, 35]. For the surface binding energies of Si and Ge atoms in the $\mathrm{Si}_c\mathrm{Ge}_{1-c}$ alloy we use a simple model based on a pair-interaction picture [36, 37]:

$$U_{\mathrm{Si}}(c) = cU^0_{\mathrm{Si}} + (1-c)U^{\mathrm{pureGe}}_{\mathrm{Si}} \tag{1}$$

$$U_{\mathrm{Ge}}(c) = cU^{\mathrm{pureSi}}_{\mathrm{Ge}} + (1-c)U^0_{\mathrm{Ge}} \tag{2}$$

Here, U^0_{Si} and U^0_{Ge} are the surface binding energies of the pure materials, which are approximated by the cohesive energies 4.70 eV and 3.88 eV for Si and Ge, respectively. The other energies, $U^{\mathrm{pureGe}}_{\mathrm{Si}}$ and $U^{\mathrm{pureSi}}_{\mathrm{Ge}}$, are the surface binding energies of atoms of one type on pure material of the other type and are given by

$$U^{\mathrm{pureGe}}_{\mathrm{Si}} = U^{\mathrm{pureSi}}_{\mathrm{Ge}} = \frac{1}{2}(U^0_{\mathrm{Si}} + U^0_{\mathrm{Ge}}). \tag{3}$$

The atomic density of the $\mathrm{Si}_c\mathrm{Ge}_{1-c}$ alloy is calculated assuming constant atomic volumes of Si and Ge consistent with atomic densities of pure Si and Ge of 4.994×10^{22} cm^{-3} and 4.428×10^{22} cm^{-3}, respectively. The lower surface binding energy of Ge requires that the trajectory cutoff-energy and the displacement energy are also set to this value; for a discussion see [34].

An extension of IMSIL required for this work was the implementation of a spherical geometry. This was done in a straightforward manner, basically replacing the z coordinate with the distance from the sphere center in geometry checks.

MC simulations were performed for central impacts of 20 keV Ar on $\mathrm{Si}_c\mathrm{Ge}_{1-c}$ spheres with 19 different radii between 1 and 1000 nm and on flat targets, for Si concentrations of $c = 0$, 0.25, 0.5, 0.75, and 1. The number of impacts followed in each simulation was 10^7.

B. Molecular dynamics

MD simulations are performed for small a-$\mathrm{Si}_c\mathrm{Ge}_{1-c}$ spheres with radii $R = 1$, 1.5, 2.5, and 3.5 nm. As in our MC simulations we investigate sputtering by central impacts of 20 keV Ar on a-$\mathrm{Si}_c\mathrm{Ge}_{1-c}$ mixtures with Si concentrations $c = 0$, 0.25, 0.5, 0.75, and 1.

The Si-Si interaction is modeled by the Stillinger-Weber potential [38], and the Ge-Ge interaction by a modification provided by Posselt and Gabriel [39], which uses the same potential form, but with adapted parameters. We emphasize that these potentials take care to fit the cohesive energies $U^0_{\mathrm{Si}} = 4.70$ eV and $U^0_{\mathrm{Ge}} = 3.88$ eV properly; also the melting temperatures (1687 K for Si and 1211 K for Ge) are implemented satisfactorily. We model the Si-Ge interaction by the same potential form, and using the arithmetic average of the parameters of Si and Ge, following Hossain *et al.* [40]. The Si potential is cut off at 3.77 Å, and the Ge and Si-Ge potentials at 3.93 Å. For small interaction distances the two-body part of the potential is fitted to the ZBL potential [32]. The Ar projectile interacts with Si and Ge atoms via the ZBL potential. Electronic stopping is disregarded in the MD simulations.

Bulk amorphous $\mathrm{Si}_c\mathrm{Ge}_{1-c}$ samples containing around 45,000 atoms are prepared by the recipe of Posselt and Gabriel [39], based on previous work by Luedtke and Landman [41], in a simulation cell using periodic boundary conditions. In short, crystals are heated above the melting temperature; during quenching, the 3-body term of the potential is increased in order to enhance the tendency to form tetrahedrally coordinated structures; after cooling the potential is restored again. After amorphization, the samples are relaxed by minimizing the potential energy using conjugate-gradient techniques until the samples reach near zero temperature and pressure.

In order to characterize the quality of our alloys, we calculate the near-order parameter

$$\zeta = \frac{P_{\mathrm{GeGe}} - (1-c)}{c}, \tag{4}$$

where P_{GeGe} is the probability that a Ge atom has a Ge nearest neighbor. This quantity is calculated as the average of Z_{GeGe}/N over all Ge atoms, where N is the number of nearest neighbors, and Z_{GeGe} is the number of Ge neighbors. Evidently, $\zeta = 1$ corresponds to a fully segregated alloy, and $\zeta = 0$ to a random alloy. Our mixtures are characterized by values of ζ of $-0.01 \cdots + 0.02$, corresponding to a random alloy. In addition, we verified that the number density of the alloys changes linearly between that of the pure Ge and Si spheres, in agreement with experimental data [42].

Spheres are cut out of these bulk samples and relaxed to zero temperature and pressure. For each sphere radius, 250 central impacts were simulated. The impacts differed in that in each case a different impact point was chosen at random on the sphere. Simulations are followed for 3 ps. Determination of the sputter yields of our small spheres

is complicated by fragmentation. We identify fragments as groups of atoms that are separated from each other by distances of at least the cutoff radius of the potential. All atoms which do not belong to the largest fragment are considered sputtered.

In addition, MD simulations have also been performed for a flat target at normal incidence. The target has a depth of 100 Å and a lateral extension of 100 Å × 100 Å. The lateral and bottom boundaries are damped in order to mimic energy dissipation to the surroundings. Each impact occurs on a random position in the central part (50 Å × 50 Å) of the target. For the flat targets, atoms are considered to be sputtered if they are at least twice the cutoff radius of the potential away from the original flat surface.

We compared our sputter yields for pure Si targets with those published earlier by Nietiadi *et al.* [9]; the sputter yields of spheres are smaller by about 20%, while the results for the flat target are reproduced within statistics. The reduction of the sphere yield is mainly due to our improved relaxation procedure.

III. ANALYTICAL MODEL

In this section, we will develop a model of sputtering from homogeneous targets composed of two atomic species. It is a natural extension of the Sigmund theory of sputtering from elemental materials. Our model makes predictions on the behavior of the partial sputter yields and the sputter preferentiality that will be compared with our simulation results on $\mathrm{Si}_c\mathrm{Ge}_{1-c}$ in Section IV.

We begin by considering the impact of a single ion of energy ϵ on a sphere of radius R that is composed of an elemental material. We will limit our attention to central impacts, i.e., those with an impact parameter of zero. We place the origin O at the point of impact and put the z-axis along the inward-pointing normal to the surface.

In the Sigmund theory of ion sputtering [1], the average energy density deposited at a point (x, y, z) within the solid by the random slowing down of the ion is taken to be

$$E_D(x,y,z) = \frac{\epsilon}{(2\pi)^{3/2}\alpha_e\beta_e^2}\exp\left(-\frac{(z-a_e)^2}{2\alpha_e^2} - \frac{x^2+y^2}{2\beta_e^2}\right). \quad (5)$$

Here a_e is the average depth of energy deposition, and α_e and β_e are the longitudinal and transverse straggling lengths, respectively. The contours of equal energy deposition are ellipsoids of revolution centered at the point $a_e\hat{z}$ with the z-axis as their axis of symmetry. Finally, the average number of atoms that are sputtered from a small area element dA centered on a point $\mathbf{r}$ on the sphere's surface, $n(\mathbf{r})dA$, is assumed to be proportional to the average energy deposited there:

$$n(\mathbf{r})dA = \lambda E_D(\mathbf{r})dA. \quad (6)$$

Here the sputtering efficiency λ is a constant, and so it is independent of the sphere's radius R.

We now move on to consider the case in which the sphere is composed of two completely miscible atomic species, 1 and 2. We restrict our attention to the case in which the concentration c of species 1 is independent of position within the sphere.

We will take the power deposited in the alloy to be given by a linear interpolation between the powers deposited in the pure materials [43]. Explicitly, we assume that

$$E_D(\mathbf{r}) = c_1 E^0_{D,1}(\mathbf{r}) + c_2 E^0_{D,2}(\mathbf{r}), \quad (7)$$

where $E^0_{D,i}$ is the density of deposited energy in a target composed entirely of species i, $c_1 \equiv c$, $c_2 \equiv 1-c$ and $i = 1, 2$. Following Ref. 44, we will take the distribution of deposited energy to be given by the Sigmund form for $c = 0$ and 1, i.e., we set

$$E^0_{D,i}(x,y,z) = \frac{\epsilon}{(2\pi)^{3/2}\alpha_i\beta_i^2}\exp\left(-\frac{(z-a_i)^2}{2\alpha_i^2} - \frac{x^2+y^2}{2\beta_i^2}\right) \quad (8)$$

for $i = 1$ and 2. Note that a_1, α_1 and β_1 in general differ from a_2, α_2 and β_2 and that here and in what follows, the superscript 0 indicates that the quality in question pertains to a pure material. The mean depth and the longitudinal and transverse stragglings of the energy deposition distribution Eq. (7) are then functions of c. They are given by

$$a = c_1 a_1 + c_2 a_2 \quad (9)$$

$$\alpha^2 = c_1(\alpha_1^2 + a_1^2) + c_2(\alpha_2^2 + a_2^2) - a^2 \quad (10)$$

$$\beta^2 = c_1\beta_1^2 + c_2\beta_2^2 \quad (11)$$

The energy density deposited in species i at an arbitrary point $\mathbf{r}$ within the sphere will be taken to be

$$E_{D,i}(\mathbf{r}) = c_i E_D(\mathbf{r}) \quad (12)$$

for $i = 1$ and 2. Thus, we assume that the deposited energy is divided stoichiometrically between the two atomic species at all points $\mathbf{r}$. We complete our model by assuming that the average number of atoms of species i that are sputtered from a small area element dA centered on a point $\mathbf{r}$ on the sphere's surface, $n_i(\mathbf{r})dA$, is given by

$$n_i(\mathbf{r})dA = \lambda_i E_{D,i}(\mathbf{r})dA. \quad (13)$$

Here the constant of proportionality λ_i could depend on the concentration c. It is, however assumed to be independent of the radius of the sphere, following Sigmund's assumption that λ does not depend on the geometry of the target. Our model is readily generalized to the oblique-incidence impact of an ion on a solid of arbitrary shape.

If the sputter yields of the two atomic species were stoichiometric, we would expect

$$\frac{Y_1}{Y_2} = \frac{c}{1-c}. \tag{14}$$

Hence deviations from stoichiometric sputtering can be quantified by the preferentiality of species 1 over species 2,

$$\delta \equiv \frac{Y_1}{Y_2} \cdot \frac{1-c}{c} - 1. \tag{15}$$

Positive values of δ indicate that species 1 is sputtered preferentially, i.e., it is sputtered more than would be expected if its atomic fraction alone were considered.

Integrating Eq. (13) over the surface of the sphere S and using Eq. (12), we obtain

$$Y_i = \lambda_i c_i \int_S E_D(\mathbf{r}) dA, \tag{16}$$

where $i = 1, 2$. It follows that the sputter preferentiality

$$\delta = \frac{\lambda_1}{\lambda_2} - 1 \tag{17}$$

depends on the concentration c but is independent of the sphere's radius R. This is one of the primary predictions of our model.

We will next find approximate expressions for Y_1 and Y_2 that are valid in the limit of large sphere radii R. Our starting point will be Eq. (16). Employing Eq. (7), we obtain

$$\int_S E_D(\mathbf{r}) dA = \sum_{i=1}^{2} c_i \int_S E^0_{D,i}(\mathbf{r}) dA. \tag{18}$$

Let Y_i^0 denote the sputter yield of a sphere of radius R that is composed entirely of species i. Equations (16) and (18) yield

$$Y_i^0 = \lambda_i^0 \int_S E^0_{D,i}(\mathbf{r}) dA, \tag{19}$$

where $\lambda_i^0 \equiv \lambda_i(c_i = 1)$ is the sputtering efficiency for a target of pure species i. From prior work on sputtering from elemental spheres [9, 45], we know that

$$Y_i^0 \cong Y^0_{i,\infty} \left[1 + \left(\frac{\beta_i}{\alpha_i}\right)^2 \frac{a_i}{R}\right], \tag{20}$$

for $R \gg a_i$. Here $Y^0_{i,\infty}$ denotes the yield from a target with a flat surface that is made up of species i exclusively. Rewriting Eq. (18) with the help of Eqs. (19) and (20), we obtain

$$\int_S E_D(\mathbf{r}) dA \cong \sum_{i=1}^{2} \frac{c_i Y^0_{i,\infty}}{\lambda_i^0} \left[1 + \left(\frac{\beta_i}{\alpha_i}\right)^2 \frac{a_i}{R}\right], \tag{21}$$

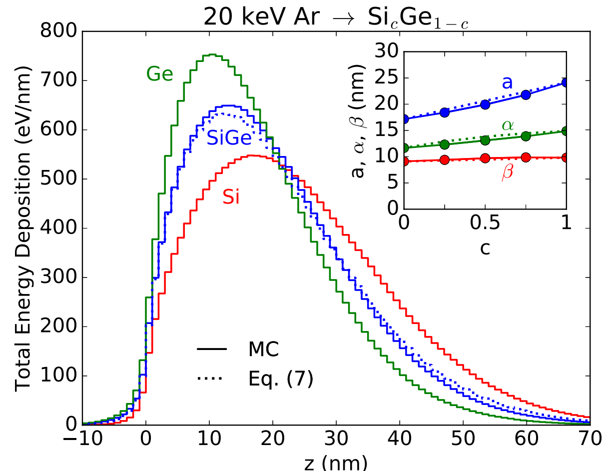

FIG. 1: MC results for the deposited energy distributions in pure Si and Ge targets and in a stoichiometric SiGe alloy; all data were obtained in an infinite medium. The behavior predicted by Eq. (7) is shown by the dotted line. The inset shows the dependence of the parameters a, α and β on Si concentration. The dotted lines here show the average depth and the longitudinal and transverse straggling lengths as given by Eqs. (9)–(11).

a result that is valid provided that R is much larger than a_1 and a_2. Let

$$\mu^0_{i,\infty} = \int_S E^0_{D,i}(\mathbf{r}) dA \tag{22}$$

for $R = \infty$, i.e., for a flat surface S. We also set $\mu_\infty = c\mu^0_{1,\infty} + (1-c)\mu^0_{2,\infty}$ and $Y_{i,\infty} = \lim_{R\to\infty} Y_i$. Using Eq. (21) in Eq. (16), we obtain our final result

$$Y_i \cong Y_{i,\infty} \left[1 + \sum_{j=1}^{2} c_j \frac{\mu^0_{j,\infty}}{\mu_\infty} \left(\frac{\beta_j}{\alpha_j}\right)^2 \frac{a_j}{R}\right], \tag{23}$$

which applies for $R \gg a_1$ and $R \gg a_2$. We conclude that for large R, the partial yield Y_i is approximately equal to its value for a flat surface plus a correction term that falls off as $1/R$. Note that Eq. (23) implies that the ratio of the partial yields and therefore the sputter preferentiality δ are approximately independent of the sphere radius R for large R, which is consistent with Eq. (17).

MC and MD tests of the Sigmund model's predictions for the sputtering of a sphere composed of an elemental material show that the model produces accurate results only for sphere radii R that are large compared to the average depth of energy deposition a [9, 45]. We therefore anticipate that our generalization of the Sigmund model to binary materials will agree with our simulations only in the limit that R is large compared to a_1 and a_2.

In Fig. 1, we show our MC results for

$$E_D(z) \equiv \int_{-\infty}^{\infty} \int_{-\infty}^{\infty} E_D(x, y, z) dx dy, \tag{24}$$

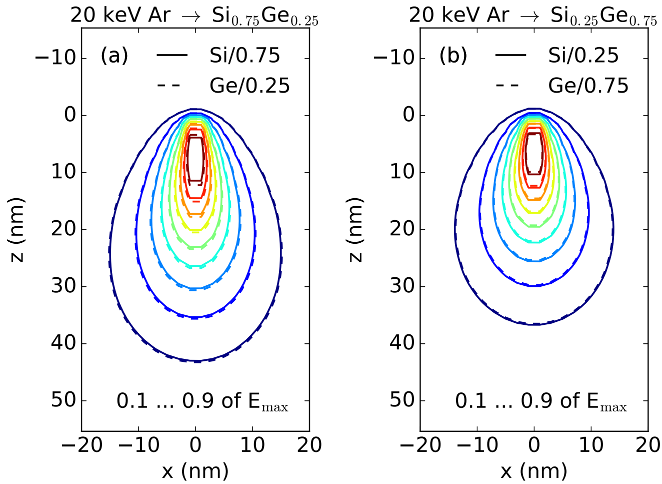

FIG. 2: Scaled deposited energy density $E_{D,i}(\mathbf{r})/c_i$ for i corresponding to Si (solid lines) and Ge (dashed lines): (a) $\mathrm{Si}_{0.75}\mathrm{Ge}_{0.25}$, (b) $\mathrm{Si}_{0.25}\mathrm{Ge}_{0.75}$. In both cases the scaled energy densities agree very well.

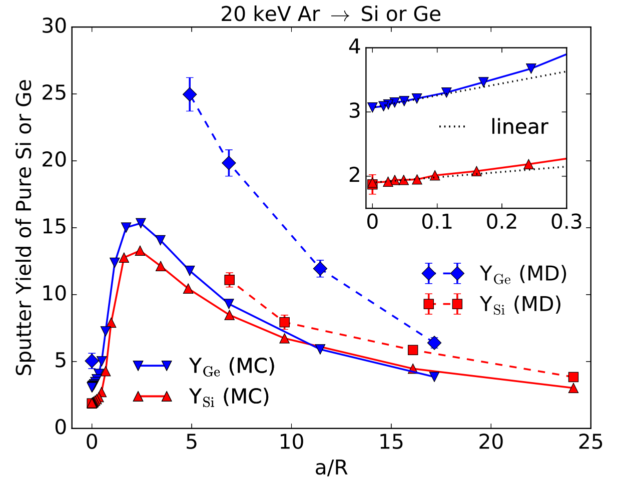

FIG. 3: Sputter yields of Si and Ge spheres (red and blue lines, respectively) as a function of inverse scaled radius a/R. Solid lines: MC results; dashed lines and symbols with error bars: MD results. In the inset the linear approximations given by Eq. (20) are depicted by the dotted lines.

for $\mathrm{Si}_c\mathrm{Ge}_{1-c}$ as a function of z for $c = 0$, 1 and 1/2, i.e., for targets composed of pure silicon, pure germanium and the stoichiometric alloy SiGe, respectively. These results were obtained for infinite targets and the ions were at the origin moving in the $+z$ direction at time $t = 0$. The dotted curve in Fig. 1 shows the linear interpolation between the $c = 0$ and $c = 1$ energy deposition profiles for $c = 1/2$. The agreement with the MC data for SiGe is quite good, and so our simulations provide support for our assumption Eq. (7).

The inset in Fig. 1 shows the MC results for the concentration dependence of the mean depth a, the longitudinal straggling α, and transverse straggling β of the deposited energy distribution. While the transverse straggling length β does not depend appreciably on concentration, the longitudinal straggling length α and even more so the depth of maximum energy deposition a increase with Si content. The dotted lines in the inset of Fig. 1 show a, α and β as given by the model's predictions Eqs. (9)–(11). Good agreement with the MC data is also seen here.

In general, cascade theory predicts that the energy deposition profiles of the two species in a binary target differ from each other [43, 46, 47]. Concrete examples of the energy partitioning, however, show only moderate deviations from stoichiometry even for extreme examples such as the hypothetical compound HfC, see e.g., Fig. 2(a) of Ref. [46]. The spatial dependence of the energy deposition profiles of the two species in a mixture has not been reported before to our knowledge.

According to Eq. (12), the energies deposited in each atom of species 1 and 2 are the same on average at an arbitrary point $\mathbf{r}$ in the solid. Equation (12) implies that

$$\frac{E_{D,1}(\mathbf{r})}{c} = \frac{E_{D,2}(\mathbf{r})}{1-c}. \tag{25}$$

Our Monte Carlo results for energy deposition in $\mathrm{Si}_c\mathrm{Ge}_{1-c}$ shown in Fig. 2 reveal that Eq. (25) and hence the assumption (12) are excellent approximations for $c = 0.25$ and 0.75. A more careful examination of Fig. 2 shows that in the Si-rich alloy, the energy deposition into Si recoils is slightly understoichiometric, i.e., $E_{D,\mathrm{Si}}/c < E_{D,\mathrm{Ge}}/(1-c)$, while the reverse is true for the Ge-rich alloy.

In theories of the pattern formation on binary materials that is induced by bombardment with a noble gas ion beam, the composition of the solid has so far been assumed to have a negligible effect on the collision cascades [26–28]. The dependence of the deposited energy distribution on c is not negligible, however, as shown by Fig. 1. The same assumption has generally been made in theories of the ion-induced pattern formation that occurs when an initially elemental solid is bombarded with a noble gas ion beam and impurities are concurrently deposited [48–51]. A recent exception to this rule may be found in Ref. [44]. There, for $0 < c < 1$, $E_D(\mathbf{r})$ was taken to be given by the linear interpolation (7).

IV. RESULTS

A. Sputter Yields

Figure 3 shows the sputter yields of the pure targets as a function of the inverse radius scaled with the respective average energy deposition depths, a/R. The qualitative behavior of the sputter yields is the same as that found for Si spheres in Ref. 9: Starting from their values for a flat target ($R = \infty$, $a/R = 0$), the yields increase with decreasing R (increasing a/R); this behavior has been proven to be due to the fact that the energy deposition

not only leads to backward sputtering in the vicinity of the ion impact point but also to lateral and even forward sputtering. Beyond a maximum at $R \sim a/2$ ($a/R \sim 2$), the yields decrease again; this decrease is due to the fact that the energy deposited in the sphere decreases and so does the available surface area.

The sputter yields for the pure Si spheres are about 30% larger for the MD results as compared to the MC results; this is qualitatively consistent with our previous findings [9], but is less pronounced. The reason for the mitigation of the discrepancy between MD and MC compared to Ref. 9 are reduced MD values due to our improved relaxation procedure, see Sect. II B. As discussed in [9], the main reason for the discrepancy is the establishment of collision spikes in the target spheres, which increase the sputter yield beyond that of linear collision cascades and hence above the values obtained by MC. Note that for the flat target, the MD and MC results agree almost perfectly, see the data point for $a/R = 0$ in the inset of Fig. 3. Near-perfect agreement between MD and MC results has also been found for Si membranes [35]. It seems that the more confined situation of bulk Si and Si membranes compared to spheres counteract target fragmentation due to spikes.

Figure 3 demonstrates that the spike effect is even more pronounced for pure Ge spheres; in this case, the MD results exceed the sputter yields obtained by MC by a factor of about 2. For the flat target ($a/R = 0$) the ratio of the Ge sputter yields is slightly smaller (~ 1.64), confirming that spikes affect the sputter yield more distinctly in the case of the nanospheres. The larger influence of spikes in Ge targets is plausible, since (i) Ge is heavier than Si, and hence the energy deposition is more localized, as evidenced in Fig. 1; (ii) Ge has a smaller melting temperature and a lower surface binding energy than Si. Both features favor the formation of collision spikes and sputtering by them [43, 52]. This holds for nanospheres as well as for flat targets as shown in Fig. 3.

The inset of Fig. 3 shows the behavior of the sputter yields for small curvatures. Here, the linear approximation Eq. (20) with parameters a_i, α_i, β_i taken from infinite-medium MC simulations, is shown for comparison by dotted lines. It is a near perfect fit for $R > 10a$ ($a/R < 0.1$) and still quite reasonable for $R > 4a$ ($a/R < 0.25$), for both Si and Ge. This result is remarkable, since Eq. (20) was derived using the ellipsoidal approximation Eq. (5), while the true energy deposition distribution functions are narrower in the lateral direction near the surface than deeper in the bulk, as exemplified by Fig. 2 for $Si_{0.75}Ge_{0.25}$ and $Si_{0.25}Ge_{0.75}$.

The results for a-Si_cGe_{1-c} mixtures are qualitatively the same and quantitatively between the results for pure Si and Ge spheres. Fig. 4 demonstrates this by showing the sputter emission from 3.5 nm radius Si_cGe_{1-c} spheres with varying Si content c; in order to emphasize the changes, the impact events leading to the most abundant sputtering are plotted. The trend toward increasingly pronounced emission, accompanied by crater formation in the target sphere and cluster emission, with increasing Ge content is clearly visible.

In Fig. 5 we show the so-called component sputter yields Y_i/c_i [24] for $Si_{0.75}Ge_{0.25}$, $Si_{0.5}Ge_{0.5}$, and $Si_{0.25}Ge_{0.75}$ spheres as obtained from our MC simulations. The component sputter yields would be identical for Si and Ge if sputtering were stoichiometric, see Eq. (14). They follow the same trends as a function of a/R as the sputter yields from the elemental targets (Fig. 3). In Fig. 5 the sphere radii R are scaled with the energy deposition depths a as obtained from the MC simulations for the appropriate concentration c_i, see the inset of Fig. 1.

The MC results for small surface curvature, $a/R < 0.3$, are displayed in the insets of Fig. 5. Note that for $a/R \lesssim 0.1$ the sputter yields are well approximated by the model prediction Eq. (23) shown by the dotted lines. Above that value, the MC data exceed the prediction indicating the importance of quadratic terms in the expansions of the partial yields in powers of a/R. In Eq. (23) we have taken a_i, α_i, β_i, and $\mu^0_{i,\infty}$ from simulations in an infinite medium, and $Y_{i,\infty}$ from flat target simulations. It is remarkable that Eq. (23) predicts the slopes of the linear approximation correctly.

B. Sputter preferentiality

For an alloy, the sputter preferentiality is of interest. The sputter preferentiality determines whether the surface concentrations deviate from the bulk values upon prolonged ion bombardment [23–25]. In agreement with Eq. (15), we denote the sputter preferentiality (of Si over Ge) by

$$\delta = \frac{Y_{\mathrm{Si}}}{Y_{\mathrm{Ge}}} \cdot \frac{1-c}{c} - 1. \qquad (26)$$

A positive value of δ indicates that Si is sputtered preferentially, i.e., more than according to its atomic fraction in the sphere. Eq. (26) also implies that Si is sputtered preferentially if the component sputter yield of Si, Y_{Si}/c, exceeds that of Ge, $Y_{\mathrm{Ge}}/(1-c)$. Therefore, according to Fig. 5, Si always sputters preferentially from our Si_cGe_{1-c} spheres.

The MC results for the sputter preferentiality δ are displayed in Fig. 6. Note that the values of δ are always positive. This means that Si always sputters preferentially from our Si_cGe_{1-c} spheres. In the range $R \gtrsim 2a$ ($a/R \lesssim 0.5$), δ is nearly independent of curvature in reasonable agreement with our model's prediction that δ does not depend on R; however, with the statistics provided in Fig. 6, a slight decrease of δ for the Si-rich alloy and a slight increase for the Ge-rich alloy may be discerned. Considering the relationship between sputter preferentiality δ and the sputtering efficiencies λ_i, Eq. (17), it may be concluded that our assumption made in Sect. III, that the sputtering efficiencies do not depend on geometry, is only valid for small curvatures, but fails

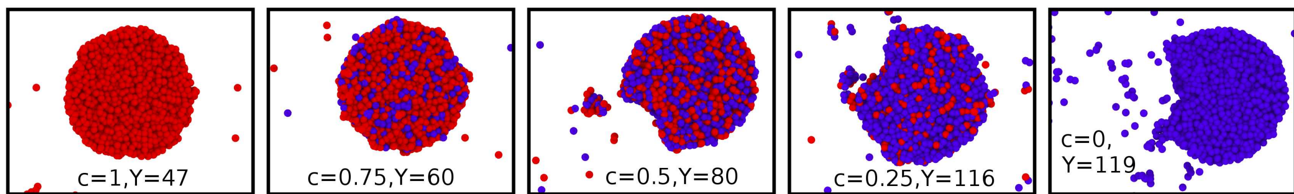

FIG. 4: Cross-sectional view through the sputtered spheres (3.5 nm radius) at 3 ps after ion impact (MD data). The impacts exhibiting the most abundant sputtering have been selected. Ions impinge along the viewing direction. Note that not all sputtered atoms are seen, as they may already have moved out of the vicinity of the sphere, they are situated in the half-space removed by the cut, or they are hidden behind the target sphere. Red: Si; blue: Ge atoms.

TABLE I: Sputter yields of a-Si_cGe_{1-c} flat targets, surface binding energies, preferentiality δ and effective power exponent m calculated by MC.

c	$Y_{\rm Si}$	$Y_{\rm Ge}$	$U_{\rm Si}$	$U_{\rm Ge}$	δ	m
0	–	3.067	4.29	3.88	–	–
0.25	0.819	1.924	4.3925	3.9825	0.278	0.164
0.5	1.407	1.051	4.495	4.085	0.338	0.185
0.75	1.768	0.416	4.5975	4.1875	0.416	0.212
1	1.901	–	4.70	4.29	–	–

for small spheres. The latter should not be too surprising given that sputtering efficiencies have been found to be different for forward and backward sputtering from membranes [35].

Theories are available for the sputter preferentiality of flat targets. Collision cascade theory shows that it depends on the ratio of the atomic masses ($M_{\rm Si} = 28.09$ amu and $M_{\rm Ge} = 72.59$ amu) and on the ratio of surface binding energies, which we determine using Eqs. (1) and (2), as [43, 53, 54]

$$\delta = \left(\frac{M_{\rm Ge}}{M_{\rm Si}}\right)^{2m} \left(\frac{U_{\rm Ge}}{U_{\rm Si}}\right)^{1-2m} - 1. \quad (27)$$

Here a parameter m enters which characterizes the low-energy behavior of the interatomic interaction; m describes a repulsive pair interaction decaying like $V(r) \propto r^{-1/m}$ for large distances r. Previous MC and MD studies [55–58] corroborated Eq. (27). For the MD studies, the parameter m has to be discussed carefully and is sometimes taken as a fitting parameter, since attractive potentials are used in MD, while m characterizes a repulsive potential; the parameter m was shown to be in the range of 0–0.2 [24].

Eq. (27) predicts that the lighter and more weakly bound species is sputtered preferentially. The atomic mass enters since the lighter species will on average deliver less energy in a collision with a heavy atom than vice versa; this is a consequence of the energy dependence of the collision cross sections. For $m = 0$, only the surface binding affects sputtering, and we expect the more weakly bound Ge to sputter preferentially. With increasing m, atomic mass becomes relevant, favoring sputtering of Si.

We assemble the MC results for flat-target sputtering in Table I. The preferentiality is somewhat stronger than what would have been expected from collision cascade theory; values of the power exponent m of around 0.2 or even larger are required to explain it from the mass and surface-binding effects, Eq. (27). Astonishingly, the preferentiality shows a distinct dependence on concentration; Si is sputtered in relatively higher proportion for the Si-rich alloys. Note that Eq. (27) predicts only a weak dependency of δ on the concentration c through the dependency of the surface binding energies on c. In our simple model based on pair-interaction binding given by Eqs. (1) and (2), the ratio $U_{\rm Si}/U_{\rm Ge}$ only varies between 1.106 for $c = 0$ and 1.096 for $c = 1$; this variation is too small to explain the pronounced dependence observed in our MC data, Table I.

Figure 6 shows that the sputter preferentiality of Si_cGe_{1-c} spheres decreases as soon as $R \lesssim 2a$ ($a/R \gtrsim 0.5$). In this case evidently the mass contribution to preferential sputtering, which is given by Eq. (27), loses its predominance, and the surface-energy term becomes more important, and the Si preferentiality is mitigated as a result.

It is difficult to obtain statistically meaningful MD data for the sputter preferentiality. The MD data show an error of the average sputter yields of around 10%; accordingly the error of the sputter yield ratio is 20%, and that of the preferentiality is of the order of the quantity itself. Combining the MD data for all concentrations ($c = 0.25$, 0.5, and 0.75) yields an average preferentiality of 0.24 ± 0.20 for flat targets and 0.18 ± 0.07 for the spheres, which agrees with the MC data shown in Fig. 6 within the (considerable) statistical errors.

Hossain *et al.* [40] used MD simulations to determine the sputter preferentiality of flat crystalline Si_cGe_{1-c} targets under 1 keV Ar impact. Even though they used only 100 impacts per target, they provided results for the sputter preferentiality; it was found to be in the range of 0.1 to 0.4 and increased with Si content. These results are in good qualitative and even semi-quantitative agreement with ours.

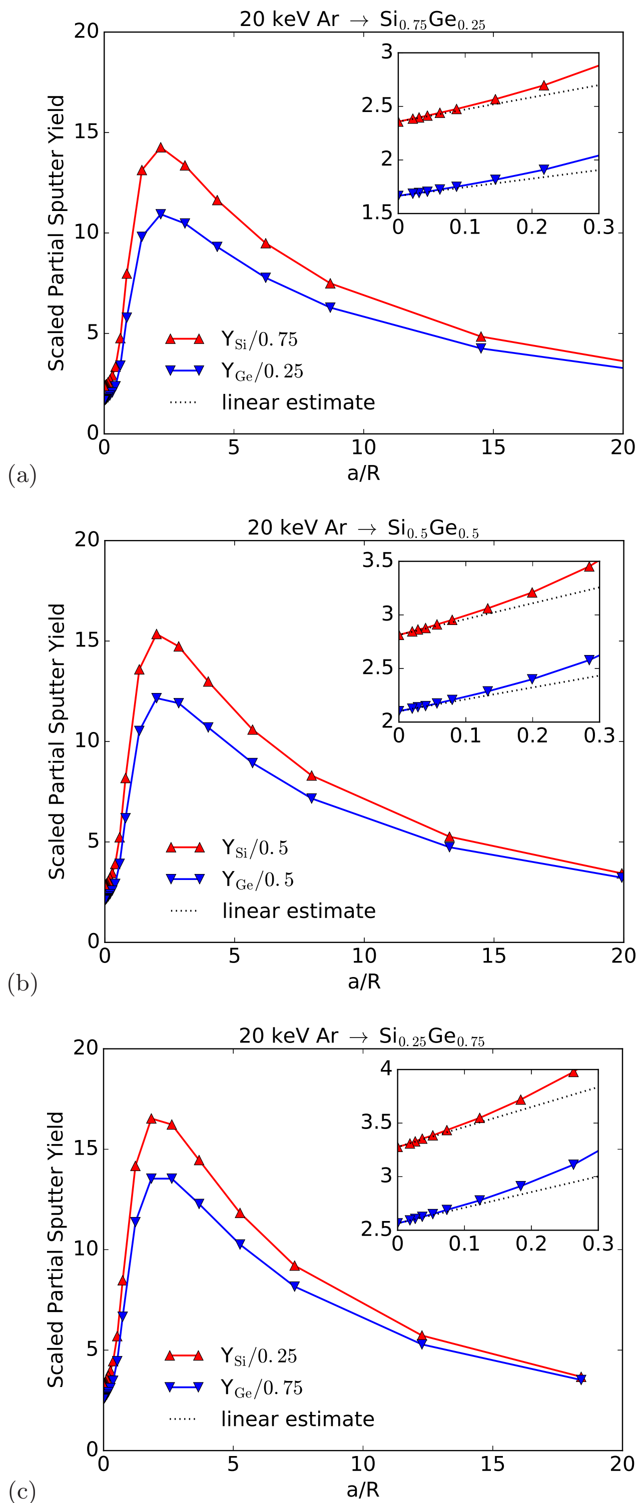

FIG. 5: MC results for the component sputter yields Y_i/c_i of Si_cGe_{1-c} spheres with (a) $c = 0.75$, (b) $c = 0.5$, (c) $c = 0.25$, as a function of the inverse reduced sphere radius a/R. The insets show the behavior for large spheres. The dotted lines show the model's predictions as given by Eq. (23).

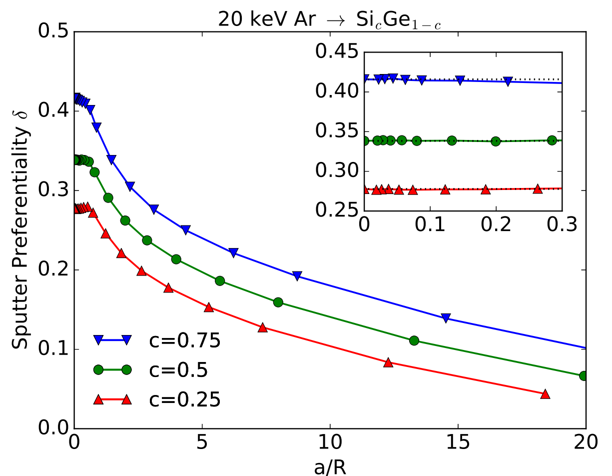

FIG. 6: MC results for the sputter preferentiality of Si_cGe_{1-c} spheres as a function of inverse reduced sphere radius a/R for $c = 0.25$, 0.5, and 0.75. In the inset the dotted lines indicate the sputter preferentiality for the flat target.

C. Sputter yield amplification

The addition of heavy atoms to a target consisting of light atoms can increase the partial sputter yield of the light atom. This phenomenon is known as sputter yield amplification [59]. For flat Si_cGe_{1-c} targets and for spheres of radius 2.5 nm, the MD data displayed in the left panel of Fig. 7(a) show that the partial sputter yield of silicon increases as we go from the pure Si target ($c = 1$) to the $Si_{0.75}Ge_{0.25}$ alloy ($c = 0.75$). Thus, these data exhibit sputter yield amplification, in contrast to the MC results shown on the right-hand side of Fig. 7(a).

Sputter yield amplification has been observed both in experiments [60, 61] and MC computer simulations [59, 60, 62, 63] of the sputtering of binary materials. The effect may be considerably stronger than the one observed by us here. The common explanation for sputter yield amplification is that the heavy ions localize the collision cascade closer to the surface; the enhanced energy deposition will thus lead to enhanced sputtering of the light species even though it is somewhat diluted.

We provide an alternative explanation here: It has been observed that in many (although not all) cases the total sputter yield is an approximately linear function of the concentration [24]. Both our MD and MC data for flat targets and nanospheres show this linearity, see Fig. 7(b). As shown in Appendix A, this implies a parabolic dependence of the partial sputter yields on the concentration if sputter preferentiality is neglected. Sputter yield amplification occurs when the maximum of the parabola for the majority material falls within the interval $0 < c < 1$. This is the case when the elemental sputter yield of the admixed material surpasses that of the original material by at least a factor of 2; in the case of preferential sputtering, the ratio of the elemental materials has to exceed $(2 + \delta)/(1 + \delta)$, see Eq. (A8).

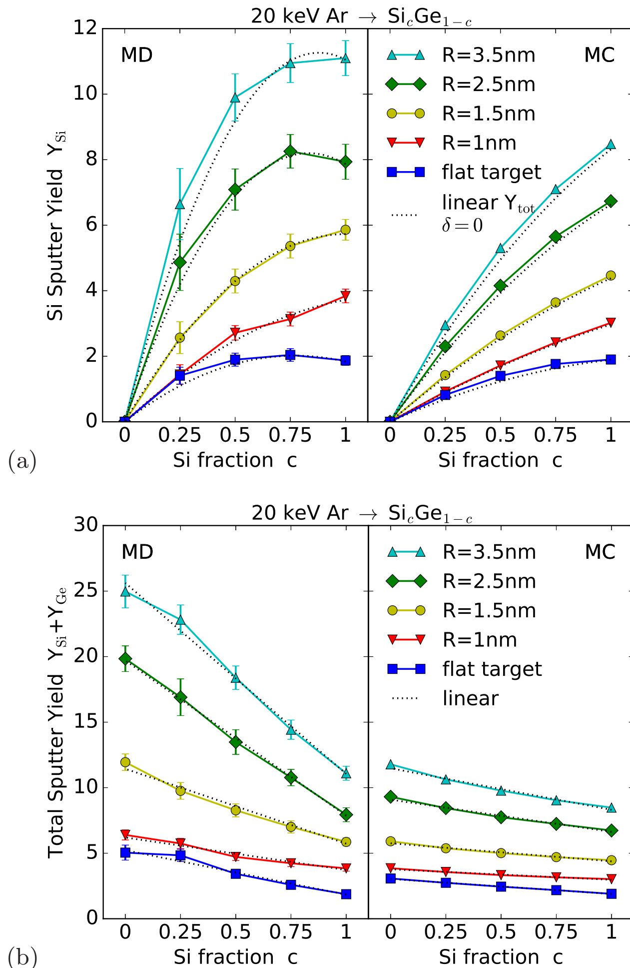

FIG. 7: (a) Partial Si sputter yield $Y_{\rm Si}$ and (b) total sputter yield $Y_{\rm tot} = Y_{\rm Si} + Y_{\rm Ge}$ as a function of Si concentration for the flat target and the four smallest nanospheres. Left: MD result, right: MC results. The dotted lines are based on linear fits to the $Y_{\rm tot}$ data and no preferentiality ($\delta = 0$).

This model explains why we do see sputter yield amplification in our MD results, but not in the MC data: Due to spike effects, for instance, the sputter yield of a flat Ge target is a factor of 2.7 larger than that of a flat Si target, thus allowing for sputter yield amplification. In MC, where spikes are not accounted for, this ratio is only 1.61, prohibiting the amplification. We note that this explanation is more general than the conventional one based on the ballistic effects of large atomic masses. On the other hand, it applies only to systems where the total sputter yield depends on the atomic concentrations linearly.

V. SUMMARY

The effect of local surface curvature on the sputtering of binary spherical targets follows that of elemental targets: the sputter yields are largest if the curvature radius is of the order of the energy deposition depth. Towards smaller curvature, the sputter yields decrease since lateral and forward sputtering no longer contribute. Towards larger curvature, on the other hand, the sputter yields shrink since the total energy deposited in the spheres decreases.

For large spheres, the curvature dependence of the sputter preferentiality δ is weak. In contrast, the preferentiality changes appreciably for high curvatures as the influence of surface binding becomes more pronounced than the mass effect.

Experimental data on sputtering of curved surfaces have been obtained primarily by bombarding nanospheres, nanorods or nanowires supported on a substrate. In a number of experiments, nanoscale objects made of an elemental material (gold) were sputtered [12, 16, 18]. Ronning *et al.*, however, have sputtered nanowires composed of the compound semiconductors ZnO and GaAs [11, 13, 14, 64]. To date, only total sputter yields have been measured. Measurements of the partial sputter yield of each atomic species that make up a given nanoscale target would be highly desirable.

Our results allow us to discuss the effect of sputter yield amplification, that is the increase in the partial sputter yield of a species with decreasing concentration of the element. For SiGe targets, it occurs for Si in Si-rich targets, and is caused by the effects of spikes induced by the admixture of the heavier Ge atoms. A simple model shows that more generally the effect occurs if the elemental sputter yield of the admixed material surpasses that of the original material by at least a factor of $(2+\delta)/(1+\delta)$.

Acknowledgments

One of us (R.M.B.) thanks the National Science Foundation for its support through grant DMR-1508745.

Appendix A: A model for sputter yield amplification

Both our MC and MD simulation results shown in Fig. 7 indicate that the total sputter yield of the Si$_c$Ge$_{1-c}$ alloy changes linearly with concentration c, i.e.,

$$Y_{\rm Si} + Y_{\rm Ge} = cY^0_{\rm Si} + (1-c)Y^0_{\rm Ge}, \tag{A1}$$

where the superscript '0' denotes the sputter yields of the elemental targets. Linearity of the sputter yield, Eq. (A1), also follows from the linearity of energy deposition, Eq. (7), if sputter preferentiality is neglected (so that $\delta = 0$) and if the sputter efficiencies λ_i are assumed to be independent of c. To see this, we begin by noting that Eq. (16) yields

$$Y_{\rm Si} + Y_{\rm Ge} = [\lambda_{\rm Si}c + \lambda_{\rm Ge}(1-c)] \int_S E_D(\mathbf{r})dA. \tag{A2}$$

According to Eq. (17), if the sputter preferentiality δ is zero, then $\lambda_{\rm Si} = \lambda_{\rm Ge}$ and Eq. (A2) becomes

$$Y_{\rm Si} + Y_{\rm Ge} = \lambda_{\rm Si} \int_S E_D(\mathbf{r}) dA, \tag{A3}$$

and linearity of $Y_{\rm Si} + Y_{\rm Ge}$ in c follows from the linearity of $E_D(\mathbf{r})$ if $\lambda_{\rm Si} = \lambda_{\rm Ge}$ is independent of c.

Previous simulations of 1 keV Ar impact on a flat $\mathrm{Si}_c\mathrm{Ge}_{1-c}$ alloy surface exhibit a quadratic, rather than linear, dependence of the total sputter yield on c [40]. However, this appears to have been caused by the poor statistics in these simulations; the total yields we calculated with our MC code – both for 1 keV and 20 keV impact energy – as well as our MD results for 20 keV were found to depend linearly on c.

We now assume Eq. (A1) to also hold for $\delta \neq 0$, as indicated by our MC and MD results. Recalling the definition of the preferentiality δ given in Eq. (26), we can eliminate the Ge sputter yield,

$$Y_{\rm Ge} = \frac{1-c}{c} \frac{1}{1+\delta} Y_{\rm Si} \tag{A4}$$

from Eq. (A1) and so obtain

$$\frac{Y_{\rm Si}}{Y^0_{\rm Si}} = \frac{1+\delta}{1+c\delta} \left[c^2 + c(1-c)r \right], \tag{A5}$$

where r denotes the sputter yield ratio of the pure elements:

$$r = \frac{Y^0_{\rm Ge}}{Y^0_{\rm Si}}. \tag{A6}$$

For $\delta = 0$, $Y_{\rm Si}/Y^0_{\rm Si}$ is a quadratic function of c, and it displays a close resemblance to our simulation result, as seen in Fig. 7(a).

Sputter yield amplification occurs if the sputter yield of Si increases while its concentration decreases, i.e.,

$$\left. \frac{\mathrm{d}\, Y_{\rm Si}}{\mathrm{d}\, c} \right|_{c=1} < 0. \tag{A7}$$

Using Eq. (A5), we find that this is the case if

$$r > \frac{2+\delta}{1+\delta} = 2 - \delta + O(\delta^2), \tag{A8}$$

where the expansion holds for $|\delta| \ll 1$. Here the preferentiality of the (almost) pure material, $\delta(c \to 1)$, applies. It may be shown that given Eq. (A1) holds, Eq. (A8) even holds if the sputter preferentiality depends on the concentration, i.e., $\delta = \delta(c)$.

We conclude that the assumption of a linear change of the total sputter yield with concentration, Eq. (A1), predicts a sputter yield amplification effect for $r > 2$ in the case of vanishing preferentiality. If Si is preferentially sputtered, $\delta > 0$, the amplification effect occurs for even smaller sputter yield ratios r.

[1] P. Sigmund, J. Mater. Sci. **8**, 1545 (1973).

[2] R. M. Bradley and J. M. E. Harper, J. Vac. Sci. Technol. A **6**, 2390 (1988).

[3] R. Kissel and H. M. Urbassek, Nucl. Instrum. Meth. B **180**, 293 (2001).

[4] R. Kissel and H. M. Urbassek, Int. J. Mass Spectrom. **208**, 29 (2001).

[5] S. Zimmermann and H. M. Urbassek, Int. J. Mass Spectrom. **272**, 91 (2008).

[6] T. T. Järvi, J. A. Pakarinen, A. Kuronen, and K. Nordlund, Europhys. Lett. **82**, 26002 (2008).

[7] T. T. Järvi and K. Nordlund, Nucl. Instrum. Meth. B **272**, 66 (2012).

[8] J. C. Jimenez-Sanz, A. M. C. Perez-Martin, and J. J. Jimenez-Rodriguez, Nucl. Instrum. Meth. B **316**, 210 (2013).

[9] M. L. Nietiadi, L. Sandoval, H. M. Urbassek, and W. Möller, Phys. Rev. B **90**, 045417 (2014).

[10] L. Sandoval and H. M. Urbassek, Nanoscale Res. Lett. **10**, 314 (2015).

[11] C. Ronning, C. Borschel, S. Geburt, and R. Niepelt, Mat. Sci. Eng. R **70**, 30 (2010).

[12] G. Greaves, J. A. Hinks, P. Busby, N. J. Mellors, A. Ilinov, A. Kuronen, K. Nordlund, and S. E. Donnelly, Phys. Rev. Lett. **111**, 065504 (2013).

[13] A. Johannes, S. Noack, W. Paschoal Jr., S. Kumar, D. Jacobsson, H. Pettersson, L. Samuelson, K. A. Dick, G. Martinez-Criado, M. Burghammer, et al., J. Phys. D **47**, 394003 (2014).

[14] A. Johannes, S. Noack, W. Paschoal Jr., S. Kumar, D. Jacobsson, H. Pettersson, L. Samuelson, K. A. Dick, G. Martinez-Criado, M. Burghammer, et al., J. Phys. D **48**, 079501 (2015).

[15] H. M. Urbassek, R. M. Bradley, M. L. Nietiadi, and W. Möller, Phys. Rev. B **91**, 165418 (2015).

[16] J. A. Hinks, F. Hibberd, K. Hattar, A. Ilinov, D. C. Bufford, F. Djurabekova, G. Greaves, A. Kuronen, S. E. Donnelly, and K. Nordlund, Sci. Rep. **8**, 512 (2018).

[17] T. T. Järvi, D. Pohl, K. Albe, B. Rellinghaus, L. Schultz, J. Fassbender, A. Kuronen, and K. Nordlund, Europhys. Lett. **85**, 26001 (2009).

[18] A. Klimmer, P. Ziemann, J. Biskupek, U. Kaiser, and M. Flesch, Phys. Rev. B **79**, 155427 (2009).

[19] A. V. Krasheninnikov and K. Nordlund, J. Appl. Phys. **107**, 071301 (2010).

[20] U. Kirchner, R. Vogt, C. Natzeck, and J. Goschnick, J. Aerosol Sci. **34**, 1323 (2003).

[21] A. Bouchoule, Phys. World **6**, 47 (1993), no. 8.

[22] M. P. Harrison and R. M. Bradley, Phys. Rev. B **89**, 245401 (2014).
[23] H. H. Andersen, in *Ion Implantation and Beam Processing*, edited by J. S. Williams and J. M. Poate (Academic, Sydney, 1984), p. 127.
[24] G. Betz and G. K. Wehner, in *Sputtering by Particle Bombardment II*, edited by R. Behrisch (Springer, Berlin, 1983), vol. 52 of *Top. Appl. Phys.*, pp. 11–90.
[25] M. Nastasi and J.W. Mayer, *Ion Implantation and Synthesis of Materials* (Springer Berlin Heidelberg, 2006).
[26] V. B. Shenoy, W. L. Chan, and E. Chason, Phys. Rev. Lett. **98**, 256101 (2007).
[27] R. M. Bradley and P. D. Shipman, Phys. Rev. Lett. **105**, 145501 (2010).
[28] P. D. Shipman and R. M. Bradley, Phys. Rev. B **84**, 085420 (2011).
[29] S. Facsko, T. Dekorsy, C. Koerdt, C. Trappe, H. Kurz, A. Vogt, and H. L. Hartnagel, Science **285**, 1551 (1999).
[30] G. Hobler, Nucl. Instrum. Meth. B **96**, 155 (1995).
[31] C. Ebm and G. Hobler, Nucl. Instrum. Meth. B **267**, 2987 (2009).
[32] J. F. Ziegler, J. P. Biersack, and U. Littmark, *The Stopping and Range of Ions in Solids* (Pergamon, New York, 1985).
[33] S. N. Markin, D. Primetzhofer, and P. Bauer, Phys. Rev. Lett. **103**, 113201 (2009).
[34] G. Hobler, R. M. Bradley, and H. M. Urbassek, Phys. Rev. B **93**, 205443 (2016).
[35] G. Hobler, M. L. Nietiadi, R. M. Bradley, and H. M. Urbassek, J. Appl. Phys. **119**, 245105 (2016).
[36] R. Kelly, Nucl. Instr. Meth. **149**, 553 (1978).
[37] R. Kelly, Surf. Sci. **100**, 85 (1980).
[38] F. H. Stillinger and T. A. Weber, Phys. Rev. B **31**, 5262 (1985).
[39] M. Posselt and A. Gabriel, Phys. Rev. B **80**, 045202 (2009).
[40] M. Z. Hossain, J. B. Freund, and H. T. Johnson, J. Appl. Phys. **103**, 073508 (2008).
[41] W. D. Luedtke and U. Landman, Phys. Rev. B **37**, 4656 (1988).
[42] *Electronic archive: "New semiconductor materials. Characteristics and properties"* (2018), http://www.ioffe.ru/SVA/NSM/Semicond/SiGe/basic.html.
[43] P. Sigmund, in *Sputtering by particle bombardment I*, edited by R. Behrisch (Springer, Berlin, 1981), p. 9.
[44] R. M. Bradley, J. Appl. Phys. **119**, 134305 (2016).
[45] M. L. Nietiadi and H. M. Urbassek, Appl. Phys. Lett. **103**, 113108 (2013).
[46] M. Vicanek, U. Conrad, and H. M. Urbassek, Phys. Rev. B **47**, 617 (1993).
[47] M. Vicanek and H. M. Urbassek, Nucl. Instrum. Meth. B **260**, 537 (2007).
[48] J. Zhou and M. Lu, Phys. Rev. B **82**, 125404 (2010).
[49] R. M. Bradley, Phys. Rev. B **84**, 075413 (2011).
[50] R. M. Bradley, Phys. Rev. B **85**, 115419 (2012).
[51] R. M. Bradley, Phys. Rev. B **87**, 205408 (2013).
[52] P. Sigmund, Appl. Phys. Lett. **25**, 169 (1974), erratum: ibid. **27**, 52 (1975).
[53] P. Sigmund and N. Q. Lam, Mat. Fys. Medd. K. Dan. Vidensk. Selsk. **43**, 255 (1993).
[54] N. Andersen and P. Sigmund, Mat. Fys. Medd. Dan. Vid. Selsk. **39** (1974).
[55] U. Conrad and H. M. Urbassek, Nucl. Instrum. Meth. B **61**, 295 (1991).
[56] N. Q. Lam and K. Johannessen, Nucl. Instrum. Meth. B **71**, 371 (1992).
[57] H. Gades and H. M. Urbassek, Nucl. Instrum. Meth. B **102**, 261 (1995).
[58] V. I. Shulga and P. Sigmund, Nucl. Instrum. Meth. B **119**, 359 (1996).
[59] S. Berg, A. M. Barklund, B. Gelin, C. Nender, and I. V. Katardjiev, J. Vac. Sci. Technol. A **10**, 1592 (1992).
[60] C. Nender, I. V. Katardjiev, J. P. Biersack, S. Berg, and A. M. Barklund, Radiat. Eff. Defects Solids **130-131**, 281 (1994).
[61] C. Hedlund, P. Carlsson, H.-O. Blom, S. Berg, and I. V. Katardjiev, J. Vac. Sci. Technol. A **12**, 1542 (1994).
[62] L. B. Jonsson, C. Hedlund, I. V. Katardjiev, and S. Berg, Thin Solid Films **348**, 227 (1999).
[63] T. Kubart, T. Nyberg, A. Pflug, M. Siemers, M. Austgen, D. Koehl, M. Wuttig, and S. Berg, Surf. Coat. Technol. **204**, 3882 (2010).
[64] W. Möller, A. Johannes, and C. Ronning, Nanotechnology **27**, 175301 (2016).